Dalton Transactions

ROYAL SOCIETY OF CHEMISTRY

PAPER

View Article Online
View Journal | View Issue

Cite this: *Dalton Trans.*, 2024, **53**, 13394

Theoretical exploration of single-molecule magnetic and single-molecule toroic behaviors in peroxide-bridged double-triangular $\{M^{II}_3Ln^{III}_3\}$ (M = Ni, Cu and Zn; Ln = Gd, Tb and Dy) complexes†

Amit Gharu and Kuduva R. Vignesh *

Detailed state-of-the-art *ab initio* and density functional theory (DFT) calculations have been undertaken to understand both Single-Molecule Magnetic (SMM) and Single-Molecule Toroic (SMT) behaviors of fascinating 3d–4f $\{M_3Ln_3\}$ triangular complexes having the molecular formula $[M^{II}_3Ln^{III}_3(O_2)L_3(PyCO_2)_3](OH)_2(ClO_4)_2{\cdot}8H_2O$ (with M = Zn; Ln = Dy (**1**), Tb (**2**) & Gd (**3**) and M = Cu; Ln = Dy (**4**), Tb (**5**) & Gd (**6**)) and $[Ni_3Ln_3(H_2O)_3(mpko)_9(O_2)(NO_3)_3](ClO_4){\cdot}3CH_3OH{\cdot}3CH_3CN$ (Ln = Dy (**7**), Tb (**8**), and Gd (**9**)) [mpkoH = 1-(pyrazin-2-yl)ethanone oxime]. All these complexes possess a peroxide ligand that bridges the $\{Ln^{III}_3\}$ triangle in a μ^3-η^3:η^3 fashion and the oxygen atoms/oxime of co-ligands that connect each M^{II} ion to the $\{Ln^{III}_3\}$ triangle. Through our computational studies, we tried to find the key role of the peroxide bridge and how it affects the SMM and SMT behavior of these complexes. Primarily, *ab initio* Complete Active Space Self-Consistent Field (CASSCF) SINGLE_ANISO + RASSI-SO + POLY_ANISO calculations were performed on **1**, **2**, **4**, **5**, **7**, and **8** to study the anisotropic behavior of each Ln(III) ion, to derive the magnetic relaxation mechanism and to calculate the Ln^{III}–Ln^{III} and Cu^{II}/Ni^{II}–Ln^{III} magnetic coupling constants. DFT calculations were also performed to validate these exchange interactions (J) by computing the Gd^{III}–Gd^{III} and Cu^{II}/Ni^{II}–Gd^{III} interactions in **3**, **6**, and **9**. Our calculations explained the experimental magnetic relaxation processes and the magnetic exchange interactions for all the complexes, which also strongly imply that the peroxide bridge plays a role in the SMM behavior observed in these systems. On the other hand, this peroxide bridge does not support the SMT behavior. To investigate the effect of bridging ions in $\{M_3Ln_3\}$ systems, we modeled a $\{Zn^{II}_3Dy^{III}_3\}$ complex (**1a**) with a hydroxide ion replacing the bridged peroxide ion in complex **1** and considered a hydroxide-bridged $\{Co^{III}_3Dy^{III}_3\}$ complex (**10**) having the formula $[Co_3Dy_3(OH)_4(OOCCMe_3)_6(teaH)_3(H_2O)_3](NO_3)_2{\cdot}H_2O$. We discovered that as compared to the LoProp charges of the peroxide ion, the greater negative charges on the bridging hydroxide ion reduce quantum tunneling of magnetization (QTM) effects, enabling more desirable SMM characteristics and also leading to good SMT behavior.

Received 20th June 2024,
Accepted 23rd July 2024

DOI: 10.1039/d4dt01800a

rsc.li/dalton

Introduction

Due to their bistable nature, Single-Molecule Magnets (SMMs) show various relaxation mechanisms, specifically their anisotropy barriers and quantum tunneling of magnetization (QTM).[1] SMMs display a hysteresis loop because of the slow relaxation of magnetization at low temperatures and they have many potential applications in memory storage devices and quantum computing.[2] After the discovery of the Mn_{12} compound in 1993 by Gatteschi and coworkers,[1c] various transition metal-based SMMs have been discovered; notably, $\{Mn^{III}_6\}$ and $\{Fe^{I}\}$ SMMs are well known to date with a barrier height of 86 K and 325 K, respectively.[3,4] The current record high barrier of U_{eff} = 450 cm^{-1} is held by linear two-coordinate complexes of highly anisotropic Co(II) (for example, the $Co(C(SiMe_2ONaph)_3)_2$ complex, where Naph is a naphthyl group), which is the largest for any transition metal SMMs.[5] Besides, molecules made exclusively from 4f metals show a fascinating magnetic behavior due to their significant magnetic aniso-

Department of Chemical Sciences, IISER Mohali, Sector-81, Knowledge city, S.A.S. Nagar, Mohali-140306, Punjab, India. E-mail: vigneshkuduvar@iisermohali.ac.in

†Electronic supplementary information (ESI) available: *Ab initio* CASSCF computed *g*-tensors and low-lying energy values of Ln(III) ions, structural parameters of all complexes, crystal-field parameters, POLY_ANISO simulated exchange coupled state energy values with their tunnelling gap, and the *ab initio* computed magnetic relaxation mechanism. See DOI: https://doi.org/10.1039/d4dt01800a

tropic nature, which leads to a large thermally induced energy barrier (U_{eff}). The first studied Ln-based SMM is $[TbPc_2]^-$, discovered in 2003, which was reported with an energy barrier of 230 cm^{-1} and a blocking temperature (T_B) of 1.7 K, which is very low because of the presence of quantum tunneling of magnetization within the low-lying ground and excited states.[6] Most importantly, the Dy^{III}-based complexes exhibit very high blocking temperatures without any transverse components in their ground and low-lying excited states since the uniaxial Dy(III) ions always maintain high magnitude $\pm m_J$ quantum numbers in the ground state and large separation between the ground and first excited states.[7] Recently, Dysprosium metallocene cations were discovered, which topped the race with notable advancements, achieving blocking temperatures (T_B) of up to 60 K and 80 K.[8] Radical-bridged lanthanide complexes are also in the running race to improve the SMM behavior by providing strong magnetic exchange between the radical and the Ln(III) ions.[9] In these systems, a stronger exchange coupling will help in covering the wider gap between the first excited state and the ground state. Notable radical-bridged Ln(III) examples are as follows: (i) $\{[(Me_3Si)_2N]_2(THF)Ln\}_2(\mu\text{-}\eta^2\text{:}\eta^2\text{-}N_2)^-$ (Ln = Tb, Ho, Er); among these, the strong magnetic anisotropy of Tb(III) with the effective exchange-coupling ability of the N_2^{3-} radical created the hardest molecular magnet, which exhibits magnetic hysteresis at 14 K and a 100 s blocking temperature of 13.9 K[10] and (ii) the first radical-bridged lanthanide-containing metallacycle reported by Dunbar and coworkers is $[Dy^{III}_3(hfac)_6(bptz^{\bullet-})_3]$ (hfac = 1,1,1,5,5,5-hexafluoro-2,4-pentanedionate; bptz = 3,6-bis(2-pyridyl)-1,2,4,5-tetrazine) that shows better SMM characteristics due to the presence of strong antiferromagnetic coupling (−6.62 cm^{-1}) between the radical and the Dy(III) ions.[11] The other strategy to attain strong magnetic exchange interactions, besides using radical ions, is the incorporation of 3d metals with the Ln ions, which also gives promising results.[12] The synthesis of heterometallic 3d–4f-based SMMs has provided a unique direction in the field of magnetochemistry since they possess a combination of the large spin of 3d metals and the large magnetic anisotropy of lanthanide ions.[12] Various 3d–4f complexes were reported to show excellent SMM behavior: importantly butterfly-like $[Cr^{III}_2Ln^{III}_2]$ (Ln = Tb, Dy and Ho)[13] complexes at zero-dc field having U_{eff} values in the range of 72–89 K and a blocking temperature of 3.7 K and $[Co^{III}_2Dy^{III}_2]$[14] complexes with an energy barrier of 56–117 K. Likewise, 3d–4f SMMs were reported with other 3d ions such as $Mn^{II/III/IV}$,[15] $Fe^{II/III}$,[16] $Co^{II/III}$,[14] Ni^{II},[17] Cu^{II},[18] and Zn^{II},[19]. Some notable SMMs among them are $[Mn^{III/IV}_{21}Dy^{III}]$,[15e] $[Mn^{II}_6Tb^{III}_2]$,[15f] $[Fe^{II}_2Dy^{III}]$,[16e] $[Ni^{II}_2Dy^{III}_3]$,[17c] $[Cu^{II}_6Dy^{III}_3]$,[18c] and $[Zn^{II}_2Dy^{III}]$[19c] with an energy barrier of 74 K, 103 K, 459 K, 85 K, 25 K, and 439 K, respectively. Furthermore, numerous effective 3d–4f SMMs have been reported with varaiation in the structural motifs.[12] These reported complexes show the important role of exchange interactions in quenching QTM, with longer relaxation times and butterfly-like coercive hysteresis loop opening.

On the other hand, polynuclear lanthanides with fascinating structures such as $[Dy_3]$ triangles,[20] $[Dy_4]$ squares, and planar,[21] and $[Dy_6]$ hexagons[22] show Single Molecule Toroic (SMT) properties. They are of great interest because of their high molecular symmetry, local magnetic moment, and strong intramolecular molecular interactions. SMTs are of great interest since they could be used in memory storage, quantum computing, and spintronic devices, and also because of their involvement in multiferroic materials.[23] The first $[Dy_3]$ triangle[20] and the $[Dy_6]$ hexagon[22] showed a unique SMT behavior due to the presence of strong local magnetic moment and high molecular symmetry such as S_3 and S_6, respectively, in these complexes. Toroidal magnetic behavior is observed in complexes possessing magnetic anisotropy with a non-collinear spin state. These toroidal moments were also realized when two molecular Dy(III) triangles were linked by 3d ions, which in turn provided a great opportunity to observe ferrotoroidicity, which could be used in molecular-based multiferroic materials.[24] Such a con-rotating ferrotoroidal moment in the ground state was confirmed for a series of heptanuclear $[MLn_6]$ complexes (M = Cr(III), Co(III), Fe(III), Mn(III) and Al(III); Ln = Dy^{III}, Tb^{III}, and Ho^{III} ions)[24] and another large $[Fe_{18}Dy_6]$ complex.[25] These complexes show ferrotoroidal behavior since they possess strong dipolar interactions between the $\{Dy_3\}$ triangles and S_6 symmetry.[24] If lanthanides' ground state electron density changes from prolate to oblate and *vice versa*, this may give us the expected toroidicity.[26]

In summary, most of the 3d–4f SMMs are either oxide or hydroxide-bridged complexes and only a few peroxide-bridged 3d–4f SMMs are known such as $[Zn^{II}_4Dy^{III}_7]$ with an energy barrier of 11.2 K and $[M^{II}_3Dy^{III}_3]$ (M = Zn, Cu, and Ni) with an energy barrier of 126.5 K.[27–29] SMTs with oxide or hydroxide bridges are well known, and carbonates and superoxide bridges are also limited. However, there are no SMTs with peroxide bridges. A few $\{M_3Ln_3\}$ triangles of triangles are fascinating complexes that show both SMM and SMT behaviors.[30] Thus, herein we explain how the peroxide bridges can influence SMT behavior in $\{M^{II}_3Ln^{III}_3\}$ triangles of triangles through computational calculations. The efficient and accurate theoretical description of magnetic anisotropy[30b] and its dependence on structure (magneto-structural correlations) has only recently become available, and the prediction and enforcement of structural variations in 4f/3d–4f complexes are much less developed than those of transition metal ions. We used well-established *ab initio* CASSCF/Density Functional Theory (DFT) calculations to determine the electronic ground state, magnetic exchange, magnetic relaxation pathways and a ligand field analysis involving extended Stevens's operators. A first set of complexes examined in our study have the general formula $[M^{II}_3Ln^{III}_3(O_2)L_3(PyCO_2)_3](OH)_2(ClO_4)_2{\cdot}8H_2O$ (where M = Zn; Ln = Dy (**1**), Tb (**2**) & Gd (**3**) and M = Cu; Ln = Dy (**4**), Tb (**5**) & Gd (**6**) and H_2L = *N*,*N*′-bis(3-methoxysalicylidene)-1,3-diaminopropane), and these complexes represent the first anion-orientated peroxide-bridged chiral heterometallic cluster complexes composed of achiral components, as reported by Cai-Ming Liu and coworkers.[28]

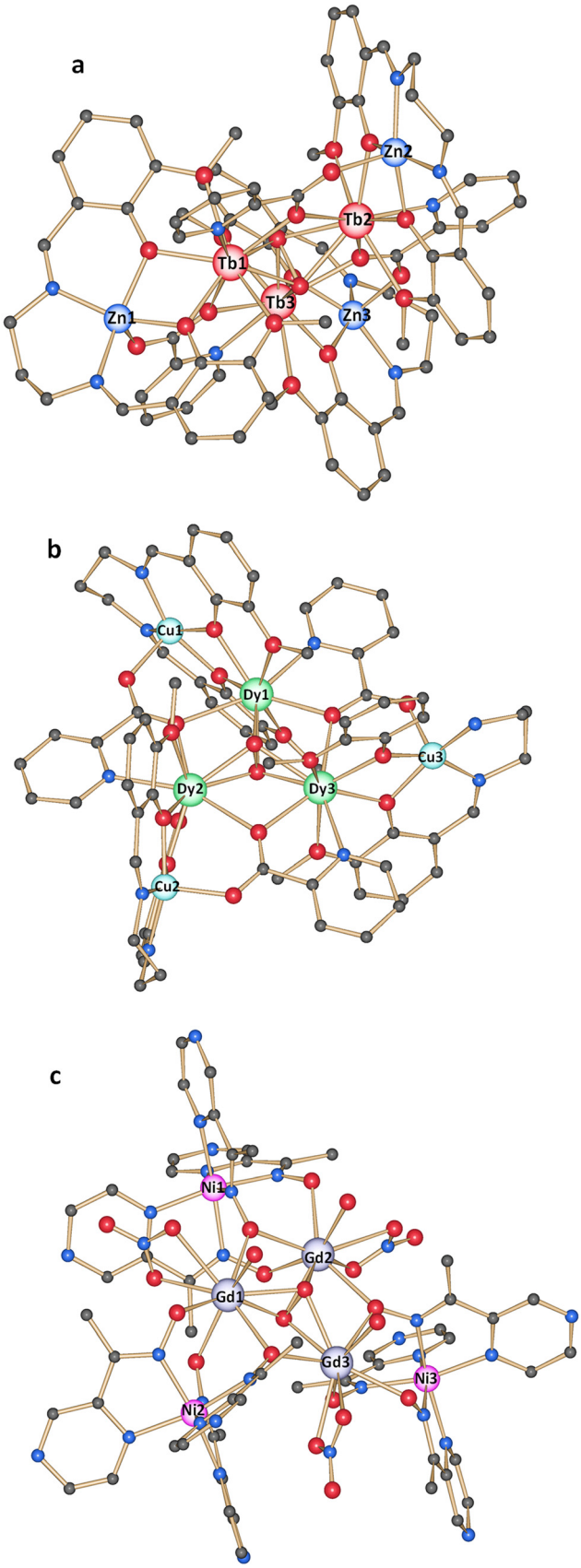

Fig. 1 Molecular structures of (a) **2**, (b) **4**, and (c) **9**.

These $\{M_3Ln_3\}$ (M = Cu, Zn; Ln = Dy, Tb, Gd) complexes are isostructural (see Fig. 1a and b) and ferromagnetic, of which $[Zn_3Dy_3(O_2)L_3(PyCO_2)_3](OH)_2(ClO_4)_2{\cdot}8H_2O$ (**1**) showed an SMM behavior under a dc field of 0.1 T, with a U_{eff} value of 126.5 K and a τ_0 value of 1.2×10^{-8} s, which is considered to be in the range of normal SMMs.[28] Similarly, the $[Zn_3Tb_3(O_2)L_3(PyCO_2)_3](OH)_2(ClO_4)_2{\cdot}8H_2O$ (**2**) complex yielded a U_{eff} value of 14.4 K and the τ_0 value is 4.3×10^{-6} s under a dc field of 0.14 T and the complex $[Zn_3Gd_3(O_2)L_3(PyCO_2)_3](OH)_2(ClO_4)_2{\cdot}8H_2O$ (**3**) exhibits a magnetocaloric effect. The next three $\{M_3Ln_3\}$ complexes contain the Cu(II) ion, in which $[Cu_3Dy_3(O_2)L_3(PyCO_2)_3](OH)_2(ClO_4)_2{\cdot}8H_2O$ (**4**) showed a field-induced SMM behavior at 0.14 T with a U_{eff} value of 25.6 K and a $\tau_0 = 1.4(0.3) \times 10^{-8}$ s. Only the $[Cu_3Tb_3(O_2)L_3(PyCO_2)_3](OH)_2(ClO_4)_2{\cdot}8H_2O$ (**5**) complex showed an SMM behavior under a zero dc field with a U_{eff} value of 31.7 K and a τ_0 value of 4.3×10^{-6} s. The Gd analog of $\{Cu_3Gd_3\}$ was not reported; however, determining the exchange interactions between the metal ions is necessary for this study. Thus, we modeled the $[Cu_3Gd_3(O_2)L_3(PyCO_2)_3](OH)_2(ClO_4)_2{\cdot}8H_2O$ complex (**6**) by replacing Dy^{3+} ions with Gd^{3+} ions and keeping the remaining atoms as such in the crystal structure of **4**.

We also examined three more $\{Ni_3Ln_3\}$ peroxide-bridged complexes reported by Xiao-Ting Wang and coworkers having the general formula $[Ln_3Ni_3(H_2O)_3(mpko)_9(O_2)(NO_3)_3](ClO_4){\cdot}3CH_3OH{\cdot}3CH_3CN$ (Ln = Dy, Tb, Gd) [mpkoH = 1-(pyrazin-2-yl)ethanone oxime].[29] The complex $[Ni_3Dy_3(H_2O)_3(mpko)_9(O_2)(NO_3)_3](ClO_4){\cdot}3CH_3OH{\cdot}3CH_3CN$ (**7**) has a U_{eff} value of 4.1 K with a relaxation time (τ_0) of 6.9×10^{-8} s under zero-dc field. The crystal structure of complex **7** was used for the modeling of the complex $[Ni_3Tb_3(H_2O)_3(mpko)_9(O_2)(NO_3)_3](ClO_4){\cdot}3CH_3OH{\cdot}3CH_3CN$ (**8**) by replacing Dy^{3+} with Tb^{3+} and keeping the other atoms in the same position, as determined by X-ray crystallography. The complex $[Ni_3Gd_3(H_2O)_3(mpko)_9(O_2)(NO_3)_3](NO_3){\cdot}10.75CH_3OH$ (**9**) has a slightly different structure and position of atoms compared to the crystal structure of complex **7**. In the $\{Ni_3Gd_3\}$ (**9**) complex, the antiferromagnetic interaction was observed between the adjacent spin states with coupling constants of $J_{Ni\cdots Ln} = -0.48$ cm^{-1} and $J_{Ln\cdots Ln} = -0.04$ cm^{-1} and it displayed a cryogenic magnetocaloric effect.

The peroxide-bridged complexes **1–9** crystallized at room temperature, which proves that these complexes are stable at room temperature.[28,29] Importantly, experimental measurements predicted that all the $\{M^{II}_3Tb^{III}_3\}$ and $\{M^{II}_3Dy^{III}_3\}$ complexes exhibit an SMM behavior with or without the dc field, with U_{eff} values ranging from 4.1 K to 126.5 K. Thus, a theoretical investigation was conducted using *ab initio* CASSCF + RASSI-SO/SINGLE_ANISO/POLY_ANISO routine calculations to try and explain these variations and offer an underlying reason for the possibility to observe SMM and SMT behaviors in these complexes. Furthermore, for complexes **3**, **6**, and **9** we performed DFT calculations to extract the isotropic exchange interactions between the Gd^{III} ions and the M^{II}–Gd^{III} ions using broken symmetry approaches.

Computational details

Ab initio calculations

For a thorough understanding of the anisotropic nature of each Ln^{III} ion and the toroidal moment of the heteronuclear $\{M^{II}_3Ln^{III}_3\}$ complexes, detailed *ab initio* calculations were performed using the MOLCAS 8.2 program.[31] The orientation of the magnetic axis for the individual lanthanide metal centers was computed by substituting the neighbouring magnetic centers with their closest diamagnetic analogue, *i.e.*, Dy^{III} and Tb^{III} ions were replaced by Lu^{III}, and Ni^{II} and Cu^{II} ions were replaced by Zn^{II} ions, based on the crystal structure data of the respective $\{M^{II}_3Ln^{III}_3\}$ complexes. The relativistic effects of Ln(III) ions were accounted for by using the Douglas–Kroll Hamiltonian,[32] and the spin-free eigenstates were obtained by complete active space self-consistent field (CASSCF) methods.[33] We used the ANO-RCC type of basis sets, *i.e.*, [ANO-RCC...8s7p5d3f2g1h] for Dy and Tb atoms, [ANO-RCC...3s2p] for C atoms,[34] [ANO-RCC...2s] for H atoms, [ANO-RCC...3s2p1d] for N and O atoms, and [ANO-RCC...5s4p2d] for Zn. Nine electrons in the seven 4f orbitals for the Dy^{3+} ions and eight electrons in the seven 4f orbitals for the Tb^{3+} ions were considered while performing CASSCF calculations. Specifically, we considered 490 doublet, 224 quartet, and 21 sextet states for the Dy^{3+} ion at the RASSI level to compute the anisotropic parameters. Likewise, we took into account 195 triplet excited states, 140 quintet excited states, and 7 septet excited states for Tb^{3+}. After computing these excited states, we performed RASSI-SO[35] calculations, which include the spin–orbit coupling, to compute the g tensors for the respective complexes. SINGLE_ANISO[36] calculations were used for computing g-tensors and also for extracting crystal field parameters. The exchange interaction between the metal ions in each Dy and Tb analogous complex was calculated by fitting their measured magnetic data using the POLY_ANISO program within the Lines model.[37]

$$\hat{H}_{ex} = -\sum_{i=1}^{3} J_i S_i S_{i+1} \quad (1)$$

here $J_i = J_i^{dipolar} + J_i^{exch}$, where J_i is the total magnetic interaction of the fitted $J_i^{dipolar}$ and J_i^{exch} parameters.

Density functional theory calculations

To calculate the magnetic exchange coupling constant (J) between the metal centers in complexes **3**, **6**, and **9**, DFT calculations were performed. We employed Noodleman's broken symmetry (BS) method to obtain the coupling constant (J) between metal centers since it provides reasonable numerical values for the Js.[38] Gaussian 16 software[39] was used to perform DFT calculations utilizing the B3LYP basis functional.[40] We used the Cundari–Stevens (CS) double-ζ basis set with effective core potential for Gd(III) ions to account for the relativistic effect of the Gd ions.[41] For the rest of the atoms, Aldrich triple-ζ basis sets were utilized.[42] The following Hamiltonians were used to assess the magnetic exchange in complexes **3** (eqn (2)), **6** (eqn (3)), and **9** (eqn (4)):

$$\hat{H} = -\left[2J_2\left(\vec{S}_{Gd1}\vec{S}_{Gd2} + \vec{S}_{Gd1}\vec{S}_{Gd3} + \vec{S}_{Gd2}\vec{S}_{Gd3}\right)\right] \quad (2)$$

$$\hat{H} = -\left[2J_1\left(\vec{S}_{Cu1}\vec{S}_{Gd1} + \vec{S}_{Cu2}\vec{S}_{Gd2} + \vec{S}_{Cu3}\vec{S}_{Gd3}\right) + 2J_2\left(\vec{S}_{Gd1}\vec{S}_{Gd2} + \vec{S}_{Gd1}\vec{S}_{Gd3} + \vec{S}_{Gd2}\vec{S}_{Gd3}\right)\right] \quad (3)$$

$$\hat{H} = \left[2J_1\left(\vec{S}_{Ni1}\vec{S}_{Gd1} + \vec{S}_{Ni2}\vec{S}_{Gd2} + \vec{S}_{Ni3}\vec{S}_{Gd3}\right) + 2J_2\left(\vec{S}_{Gd1}\vec{S}_{Gd2} + \vec{S}_{Gd1}\vec{S}_{Gd3} + \vec{S}_{Gd2}\vec{S}_{Gd3}\right)\right] \quad (4)$$

Results and discussion

All of the studied complexes possess the same topological structure where the three Ln(III) ions are arranged in a triangular fashion and bridged by a peroxide ligand. Through the carbonyl oxygen of $PyCO_2^-$ and the oxygen atom of the phenol group in **1–6** and the –NO oxygen of the 1-(pyrazin-2-yl)ethanone oxime (mpkoH) in **7–9**, the inner Ln(III) triangle is further surrounded by three transition metals, which are also arranged in a triangular fashion and form a triangle-of-triangle shaped structure for these molecules. Though all these complexes possess unique and similar topologies with a peroxide bridge, they display a different magnetic behavior due to the presence of different metal ions, which urges us to understand their electronic and magnetic properties using theoretical methods such as high-level *ab initio* CASSCF and DFT calculations (see Computational details). Initially, the magnetic relaxation mechanism, which is based on the single-ion anisotropy of the lanthanide ions in Dy(III) and Tb(III) analogues performed using the CASSCF/RASSI-SO/SINGLE_ANISO calculations are discussed. Following, how the computed orientation of the magnetic anisotropy of Dy(III) and Tb(III) ions favors/disfavors the toroidal magnetic ground state are discussed. Later, the exchange coupling between the $Ln^{III}\cdots Ln^{III}$ and $M^{II}\cdots Dy^{III}$ ions for Dy(III) and Tb(III) analogs and the magnetic relaxation mechanism based on exchange-coupled states developed using the POLY_ANISO routine employing the Lines model are discussed in detail for all the complexes. Structural parameters governing each exchange parameter are listed in Table S1.†

Single-ion anisotropy and magnetic relaxation mechanism

The single-ion calculations are performed using CASSCF/SINGLE_ANISO and the calculated anisotropic g values and the energy values of the low-lying Kramers doublets (KDs)/Ising doublets (IDs) for Ln(III) ions in complexes **1**, **2**, **4**, **5**, **7**, and **8** are listed in Tables 1 and S2–S9.†

Dy(III) analogues: 1, 4, and 7 $\{M_3Dy_3\}$. The computed energy gaps of the low-lying KDs are spanning up to ~580 cm^{-1} for all the Dy centers in **1**, ~615 cm^{-1} for all the Dy centers in **4** and ~540 cm^{-1} for all the Dy centers in **7**, which confirms that all three Dy centers are nearly identical and can reflect similar single-ion magnetic relaxation behavior in each of these complexes. The energy gap between the ground and the first

Table 1 Low-lying energies (cm^{-1}) and g-tensors of Dy^{III} fragments that originate from the corresponding ground atomic multiplets in complexes **1**, **2**, **4**, **5**, **7** and **8**

Energy									
	{Zn_3Dy_3} (**1**)			{Cu3Dy3} (**4**)			{Ni3Dy3} (**7**)		
KDs	Dy1	Dy2	Dy3	Dy1	Dy2	Dy3	Dy1	Dy2	Dy3
	0.0	0.0	0.0	0.0	0.0	0.0	0.0	0.0	0.0
	128.5	128.4	127.8	149.2	148.8	148.7	141.6	145.0	145.3
	169.7	169.6	168.8	200.1	200.8	203.2	185.9	188.1	187.0
	235.5	237.3	237.3	251.8	254.6	257.9	224.9	226.1	227.1
	351.2	354.8	352.7	349.7	354.4	356.1	295.3	296.2	296.3
	408.7	413.3	411.9	376.1	381.3	386.1	325.7	328.8	324.5
	485.0	488.0	489.1	493.5	497.1	501.8	374.1	376.9	376.5
	579.1	582.2	581.9	612.0	615.6	617.6	530.1	539.6	528.1
	g-Tensor			*g*-Tensor			*g*-Tensor		
g_x	0.000	0.000	0.000	0.000	0.000	0.000	0.005	0.005	0.005
g_y	0.003	0.003	0.003	0.002	0.002	0.002	0.006	0.006	0.005
g_z	19.688	19.688	19.712	19.619	19.623	19.654	19.451	19.516	19.478
	{Zn_3Tb_3} (**2**)			{Cu_3Tb_3} (**5**)			{Ni_3Tb_3} (**8**)		
IDs	Tb1	Tb2	Tb3	Tb1	Tb2	Tb3	Tb1	Tb2	Tb3
	0.0	0.0	0.0	0.0	0.0	0.0	0.0	0.0	0.0
	0.01	0.01	0.01	0.02	0.03	0.02	0.6	0.6	0.6
	178.4	177.6	177.1	173.4	171.8	172.3	84.3	82.8	83.1
	179.3	178.4	177.9	173.7	172.1	172.5	90.6	88.8	88.8
	324.2	323.0	322.1	319.7	317.4	318.3	158.5	159.0	158.6
	337	335.7	336.0	331.9	330.4	330.4	180.3	180.3	179.2
	427.2	427.2	425.1	425.4	422.2	424.8	239.8	240.2	239.1
	432.1	430.7	431.6	439.6	440.0	438.4	289.2	289.1	286.6
	472.6	472.1	469.3	478.0	475.5	477.2	315.7	316.1	313.7
	498.7	498.7	498.9	538.3	540.2	539.6	366.8	364.8	363.6
	509.5	509.0	507.7	548.8	548.6	549.5	372.9	371.0	369.9
	601.2	603.5	604.5	576.7	579.7	578.3	456.2	456.9	450.2
	603.7	605.8	606.9	582.0	584.2	583.3	456.9	457.8	450.9
	g-Tensor			*g*-Tensor			*g*-Tensor		
g_x	0.0000	0.0000	0.0000	0.0000	0.0000	0.0000	0.0000	0.0000	0.0000
g_y	0.0000	0.0000	0.0000	0.0000	0.0000	0.0000	0.0000	0.0000	0.0000
g_z	17.908	17.908	17.914	17.891	17.923	17.927	17.434	17.421	17.446

excited states of the Dy(III) ions are in the range of 127.8–128.5 cm^{-1} for **1**, 148.7–149.2 cm^{-1} for **4**, and 141.6–145.3 cm^{-1} for **7**. To derive the magnetic relaxation mechanism, the low-lying KDs for complexes **1**, **4**, and **7** are arranged according to their values of transition magnetic moment between the KDs, and their relaxation mechanisms are shown in Fig. 2a–c and Fig. S2–S7.† It was observed that the QTM between the ground KDs is in the range of 0.00057–0.00066μ_B for the Dy ions in **1**, 0.00037–0.00045μ_B for the Dy ions in **4**, and 0.0018–0.0019μ_B for the Dy ions in **7**, which are negligible and allow the magnetization to relax in the excited states. The observed small QTM value for all the Dy ions is attributed to the highly pure magnetic ground state of $m_J = \pm 15/2$. Furthermore, the thermally assisted QTM (TA-QTM) between the first excited states is found to be large with values in the range of 0.32–0.34μ_B in **1**, 0.12–0.14μ_B in **4**, and 0.20–0.21μ_B in **7**. These TA-QTM values confirm that the single-ion magnetic relaxation can likely occur *via* the first excited state and lead to an energy barrier of ~125 cm^{-1} for **1**, ~149 cm^{-1} for **4**, and ~145 cm^{-1} for **7**. These values confirm that these complexes could show their SMM behavior under a zero-dc field or a small applied dc field, which agrees with their experimental results. The presence of smaller QTM for all Dy ions in **1**, **4**, and **7** was further rationalized by computing the crystal field (CF) parameters. The Hamiltonian used for the CF parameters is shown in eqn (5).

$$\hat{H}_{CF} = \sum \sum_{k=-q}^{q} B_q^k \tilde{O}_k^q \quad (5)$$

According to the above crystal-field Hamiltonian equation, the QTM effects are dominant in a system where the nonaxial B_q^k (in which $q \neq 0$ and $k = 2, 4, 6$) terms are larger than the axial terms (in which $q = 0$ and $k = 2, 4, 6$).[14] The computed CF parameters for complexes **1**, **4**, and **9** are given in Tables S10–S12 in the ESI.† It is evident that the axial terms are large enough to quench the QTM in the ground state for all the Ln(III) single-ions and allow the magnetization to go further and relax in the excited states, which corroborates the observed single-ion relaxation mechanism.

Tb(III) complexes: 2, 5, and 8 {M_3Tb_3}. The computed energy gaps of the low-lying IDs for all the Tb centers are spanning up to ~604 cm^{-1} in **2**, ~582 cm^{-1} in **5**, and ~583 cm^{-1} in **8**, which confirms that they are also equal and can reflect similar single-ion magnetic relaxation behavior. The energy gaps between the first excited and the ground state for the low-lying IDs for complexes **2**, **5**, and **8** are ~178 cm^{-1}, ~173 cm^{-1}, and ~83 cm^{-1}, respectively. However, the magnetic relaxation

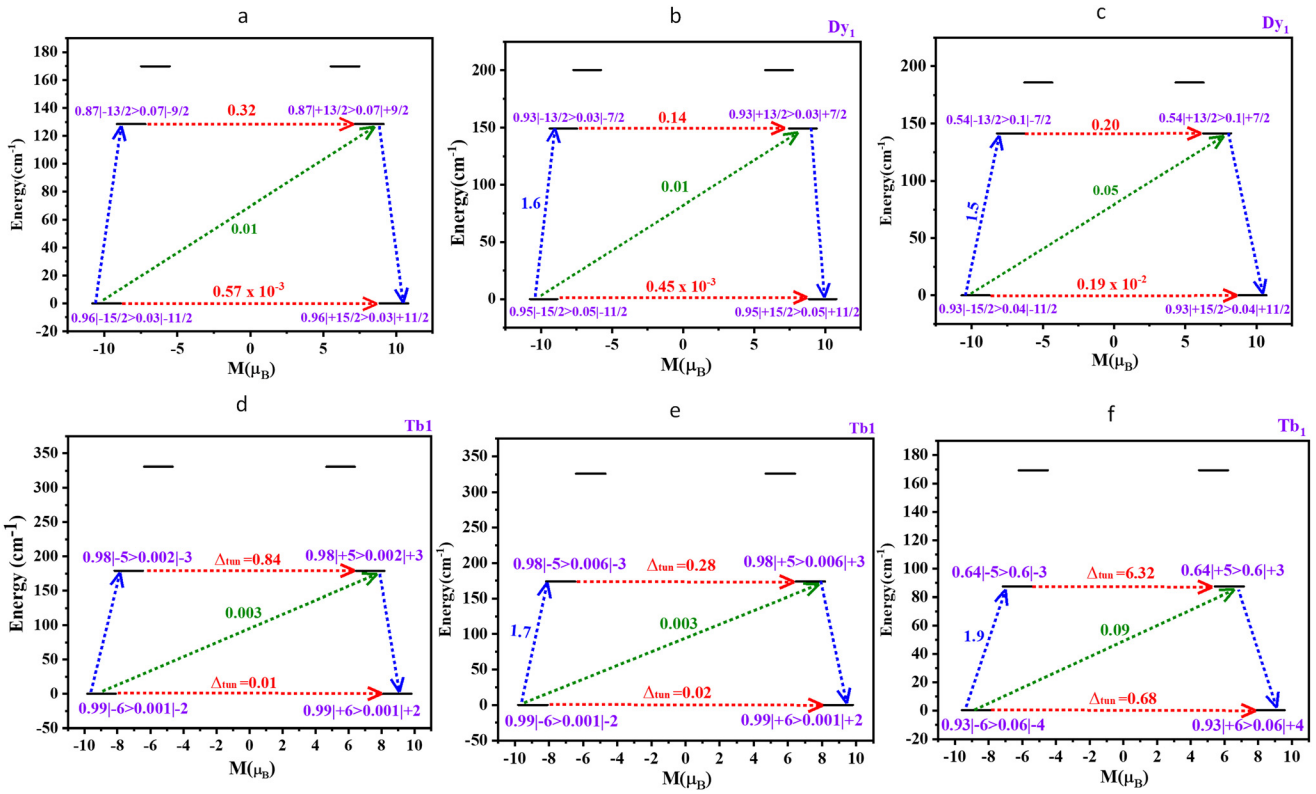

Fig. 2 Mechanism of magnetic relaxation of Dy1 and Tb1 sites in complexes (a) **1**, (b) **4**, (c) **7**, (d) **2**, (e) **5** and (f) **8**. The thick black lines indicate Kramer doublet/Ising doublet (KD/ID) states as functions of the computed magnetic moment. The dotted green and blue lines indicate the possible relaxation process such as Raman/Orbach relaxation. The dotted red lines indicate the QTM/tunnelling gap between the states.

occurs for all Tb centers in their ground state itself because of the presence of a large tunneling gap (Δ_{tun}), which is ~0.01 cm^{-1} in **2**, ~0.02 cm^{-1} for **5**, and ~0.6 cm^{-1} in **8**. Such a large tunneling gap could be reduced if a small dc field is applied or a strong magnetic exchange could quench it.[14] These assumptions could be rationalized by developing an exchange coupled state relaxation mechanism that is discussed below in detail.

Anisotropic and the ground state toroidal behavior. The computed g-anisotropic values also suggest that all three Dy(III) centers are the same and have a strong axial g_{zz} component with negligible transverse (g_{xx}, g_{yy}) components (see Table 1), signifying that the single-ion anisotropy can lead to the slow magnetic relaxation in all Dy(III) complexes **1**, **4** and **7**. The orientation of the anisotropic axes of each Dy(III) ion in **1**, **4**, and **7** is shown in Fig. 2. In complex **1**, all the Dy–O bonds range from 2.30 to 2.56 Å, with the Dy–$O_{peroxide}$ bonds ~2.36 Å. This μ-peroxide ligand bridges across Dy^{III} ions and forms a triangular $\{Dy_3^{III}\}$ topology, causing them to be at right angles at the Dy^{III} site. The large negative LoProp charges of μ-peroxide bridges cause the Dy^{III} ion's β-electron (spin-down) to deviate from them, reducing the electrostatic repulsion (see Fig. 3a), and allowing all three g_{zz} axes to align between the oxygen of pyridine-2-carboxylate ($PyCO_2^-$) and *N*,*N*′-bis(3-methoxysalicylidene)-1,3-diaminopropane (H_2L) ligands. Furthermore, the g_{zz} axes in Dy1 and Dy2 centers align along the β-electron density (see Fig. 3), whereas it is found that the direction of the main anisotropy axis of the Dy3 center is perpendicular to the $\{Dy_3\}$ motif. Thus, the anisotropic directions do not follow each other and this arrangement does not form any circular pattern to enable toroidal behavior in **1**. In complexes **4** and **7**, despite the μ-peroxide bridge possessing large negative LoProp charges, the g_{zz} axes of all three Dy centers deviate from the $\{Dy_3\}$ plane and align parallel to the center of the triangle; however, they do not follow each other, resulting in the absence of toroidal behavior. Although these complexes possess a $\{Dy_3\}$ triangular motif, these molecules lack SMT behavior since the g_{zz} anisotropy axes are oriented differently due to the presence of a peroxide bridge.

Similarly, the computed g-anisotropic values confirm that the three Tb(III) centers in complexes **2**, **5**, and **8** have strong axial g_{zz} components and small transverse (g_{xx}, g_{yy}) components (see Table 1). The electrostatic repulsion is the same as that in comparison to the complex **1**. Because Tb(III) is moderately more oblate than the Dy(III) metal ion, the μ-peroxide ligand bridges across Tb^{III} ions that help to form a triangular $\{Tb_3^{III}\}$ topology, which further causes the bridging to be at right angles at the Tb^{III} site. Here also the large negative LoProp charges on the peroxide oxygen deviate the Tb^{III} ion's β-electron (spin-down) and reduce the electrostatic repulsion

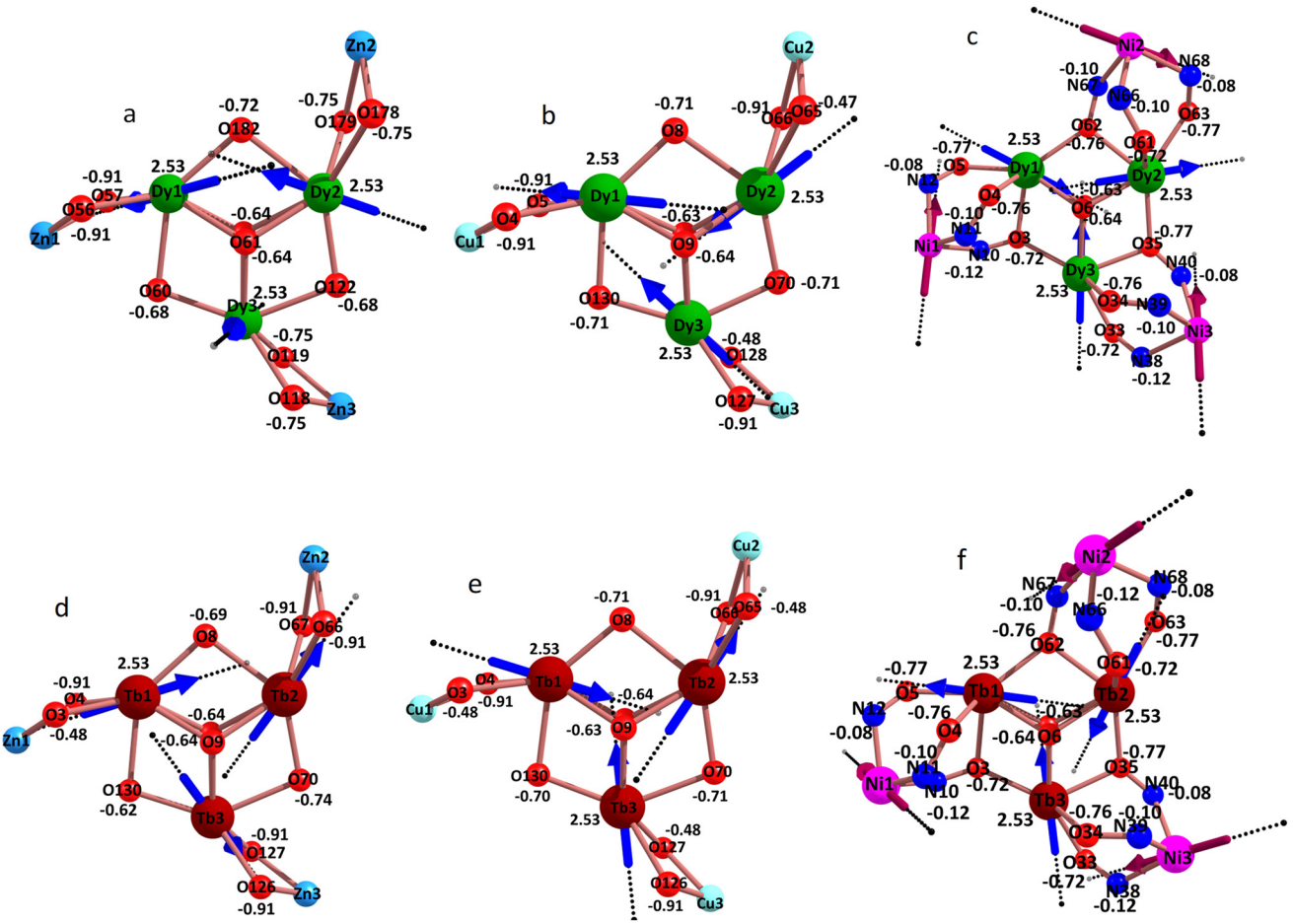

Fig. 3 LoProp charges with the anisotropic directions of Ln(III) ions for complexes (a) **1**, (b) **4**, (c) **7**, (d) **2**, (e) **5** and (f) **8**.

(see Fig. 3d), which makes the g_{zz} axes align between the oxygen of pyridine-2-carboxylate ($PyCO_2^-$) and *N*,*N*′-bis(3-methoxysalicylidene)-1,3-diaminopropane (H_2L) ligands (similar to that in complex **1**). Furthermore, the g_{zz} axis of the Tb centers is aligned along the β-electron density (see Fig. 3). These anisotropic directions do not follow each other, which indicates the absence of any toroidal behavior. In complexes **5** and **8**, the anisotropic directions are aligned parallel to the triangular $\{Tb^{III}_3\}$ topology because of the large negative LoProp charges on their μ-peroxide bridges. But the g_{zz} directions are not following each other, leading to the absence of SMT behavior. Furthermore, the paramagnetic 3d ions in these complexes do not have any significant role in influencing the toroidal behavior, since they are not directly coordinated to the peroxide ion to polarise it further.

Analysis of exchange coupled states' anisotropic energy barriers

As confirmed above, slow magnetic relaxation is possible for complexes **1**, **4**, and **7** since all the Dy^{III} ions show their single-ion anisotropic behavior, while it is not possible for Tb^{III} complexes. Thus, a polynuclear mechanism that considers the exchange coupling between the paramagnetic centers was established for all Dy and Tb analogues to obtain insight into the cluster relaxation mechanism. The exchange-coupled states' magnetic relaxation mechanism was developed by fitting the experimentally measured susceptibility data using the POLY_ANISO program with the Lines model.[37] A satisfactory fit (solid color lines) for susceptibility data (see Fig. 4) was achieved for the extracted exchange parameters which are listed in Table 2, supporting the level of theory used in our calculations. This POLY_ANISO calculation was performed using the SINGLE_ANISO computed anisotropic parameters of the Dy^{III}/Ni^{II} single ions and this strategy has been effectively used to get a good numerical estimate of the magnetic exchange parameters (J values).[11,13,14,19] The exchange Hamiltonian used to extract the J values in complexes **1**, **2**, **4**, **5**, **7**, and **8** is provided in eqn (1) in the Computational details section. Since all the complexes possess similar topology and the Ln–$O_{peroxide}$ distances and the Ln^{III}–O–Ln^{III} and Ln^{III}–O–M^{II} angles are identical (see Table S1 in ESI†), we have employed a single exchange interaction (J_1) for all Dy^{III}–Dy^{III} pairs and another exchange (J_2) for all Dy^{III}–M^{II} pairs (see the Computational details section and Fig. 5). The exchange coup-

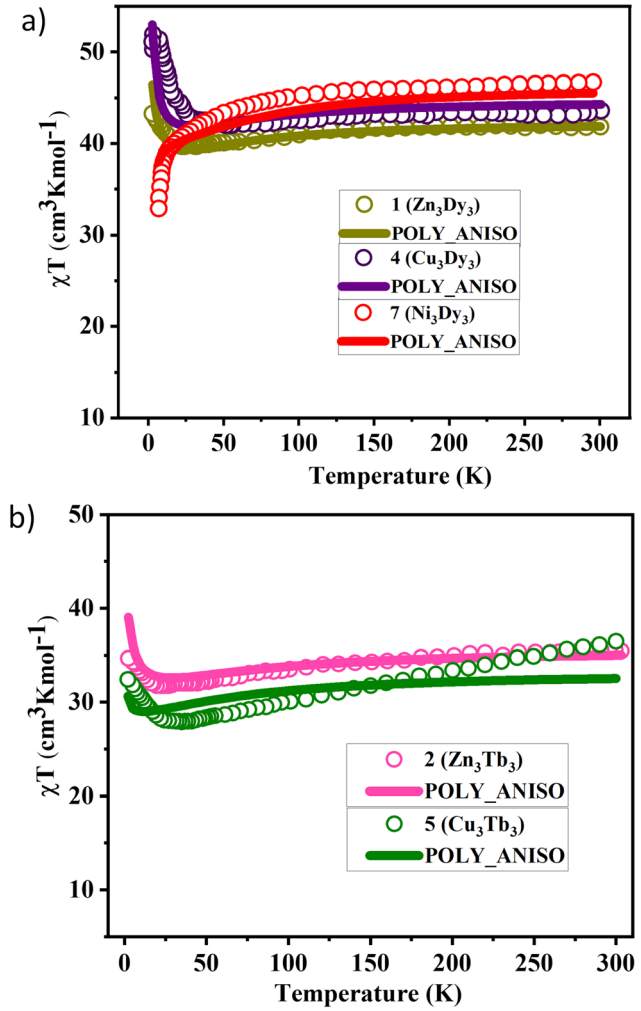

Fig. 4 POLY_ANISO fitted susceptibility data for (a) **1**, **4**, and **7** and (b) **2**, and **5**.

Table 2 POLY_ANISO computed J values (in cm^{-1}) for complexes **1**, **2**, **4**, **5**, **7**, and **8**

Complex no.	J_1	J_2	zJ
1 (Zn_3Dy_3)	0.09	—	0.01
2 (Zn_3Tb_3)	0.01	—	0.001
4 (Cu_3Dy_3)	0.06	0.8	0.001
5 (Cu_3Tb_3)	0.03	0.09	0.001
7 (Ni_3Dy_3)	0.03	−2.5	−0.01
8 (Ni_3Tb_3)	−0.02	−0.1	−0.03

ling between the spin moments of magnetic sites is described by the Lines model, within which the exchange interactions were computed.[37b]

To validate these POLY_ANISO computed J_1 and J_2 exchange interactions, we have performed detailed DFT calculations using the Gaussian 16 program by computing Gd^{III}–Gd^{III} (J_1) and Gd^{III}–M^{III} exchange coupling constants for complexes **3**, **6**, and **9**. The existing magnetic interactions in complexes **3**, **6**, and **9** are pictorially represented in Fig. 5. For example, in

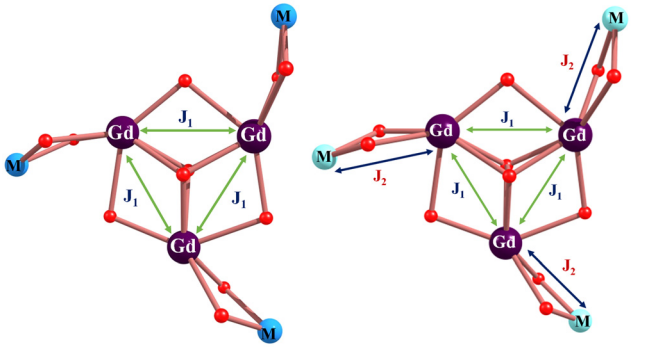

Fig. 5 Pictorial representation of the exchange interactions in complexes (left) **3** (M = Zn), (right) **6** and **9** (M = Cu/Ni).

complexes **6** and **9**, both J_1 ($Gd^{III}\cdots Gd^{III}$) and J_2 (Cu^{II}/$Ni^{II}\cdots Gd^{III}$) exchange interactions are possible, whereas J_2 does not exist in complex **3**. The DFT computed J values obtained through broken symmetry approach methods are listed in Table 3. These computed J values are in good agreement with the experimental J values and are similar to the J values derived from the Lines model (see Table 2). The J_1 ($Gd^{III}\cdots Gd^{III}$) interactions are found to be ferromagnetic in **3** and **6**. The observed ferromagnetic behavior can be rationalized through the previously established magneto-structural correlations on the $\{Gd^{III}(OR)_2Gd^{III}\}$ dimers.[43] According to this correlation study, the Gd···Gd pairs can show a ferromagnetic exchange between them when the Gd–O–Gd angle lies between 106° and 120° and they can show an antiferromagnetic exchange if the Gd–O–Gd angle decreases below 106° or increases above 120°. The average Gd^{III}–$O_{peroxide}$–Gd^{III} angle is found to be 110.5° in complexes **3** and **6** (see Table S1†) and 110° in complexes **9**, which rationalizes the observed ferromagnetic interaction between the Gd^{III} centers.

Similarly, the J_2 ($M^{II}\cdots Gd^{III}$) values are positive in complexes **6** and **9**, suggesting that the magnetic exchange is ferromagnetic for this {M–O–Gd} structural topology (where R = alkyl or aromatic groups), which is generally expected between the Gd and the transition metal complexes of the first row.[44] The spin density plots shown in Fig. S8† are used to investigate the electronic source of exchange. In all three complexes, three Gd^{III} ions were found to have a spin density of 7.027, which is more than expected, indicating that the spin polarisation mechanism is active. Since all three Gd^{III} atoms are polarising

Table 3 DFT computed J values (in cm^{-1}) of Gd(III) complexes **3**, **6**, and **9**

	DFT		Experimental[a]	
Complex no.	J_1	J_2	J_1 (cm^{-1})	J_2 (cm^{-1})
{Zn_3Gd_3} (**3**)	0.05	—	0.0008	—
{Cu_3Gd_3} (**6**)	0.3	1.02	—	—
{Ni_3Gd_3} (**9**)	0.01	−0.01	−0.04	−0.48

[a] J values taken from ref. 28 and 29.

the bridging peroxide oxygens, they have higher spin densities than ordinary oxygens, which leads to a weak ferromagnetic exchange. In complexes **6** and **9**, the spin density is delocalized between Cu(II)/Ni(II) and Gd(III) through the bridging alkoxy/oximate bridges (Fig. S8†).

The POLY_ANISO computed J values were used to determine the mechanism of the magnetic relaxation for complexes **1**, **2**, **4**, **5**, **7**, and **8**. The three Dy^{III} ions possessing ground KD states along with the three diamagnetic Zn^{II} ions and coupled antiferromagnetically with three Ni^{II} (S = 1) ions yielded a Kramers exchange spectrum in **1** and **7**, respectively, whereas the three Dy^{III} ions coupled ferromagnetically with the three Cu^{II} (S = 1/2) ions yielded a non-Kramers exchange spectrum in **4**. Similarly, the three Tb^{III} ions possessing ground Ising states along with the three diamagnetic Zn^{II} ions and coupled antiferromagnetically with three Ni^{II} (S = 1) ions yielded non-Kramers exchange coupled states in **2** and **8**, respectively; whereas the three Tb^{III} ions coupled ferromagnetically with the three Cu^{II} (S = 1/2) ions yielded Kramers exchange coupled states in **5**. Fig. 6 and Tables S13–S15† depict the spectrum of the exchange coupled states of **1**, **4**, and **7**. In complex **1**, the $Dy^{III}\cdots Dy^{III}$ interactions yielded several low-lying exchange energy levels, which reveal that the QTM/TA-QTM values are extremely small till the 6th excited states and the Raman/Orbach process value of 0.16 cm^{-1} occurring between the ±5 and ±6 transition states allowed the magnetic relaxation at this energy level, which yielded a U_{cal} of 128.3 cm^{-1} (184.6 K). Similarly, the small QTM/TA-QTM at the ground state until the 7th excited energy states yielded a U_{cal} value of 5.6 cm^{-1} (8.1 K) for complex **7** due to the Raman/Orbach process value of 0.1 cm^{-1} occurring between the ±6 and ±7 transition states. However, the extremely small tunneling gap in the ground and few excited states and the large tunneling gap of 0.7 × 10^{-4} at the 6th excited states yielded a U_{cal} value of 128.0 cm^{-1} (184.2 K) for **4**. The U_{cal} values of **1**, **4**, and **7** suggest that these complexes can show SMM behavior under a small dc field or in the absence of a dc field, which is also in good agreement with U_{eff} values of 126.5 K (at 0.1 T) and 4.1 K (at zero dc field) for **1** and **7**, respectively; however, it has been overestimated for complex **4** (U_{eff} = 25.6 K at 0.14 T).

Furthermore, for Tb analogues, the tunneling gap in the ground state is found to be moderately large for complex **2** (Δ_{tun} = 2.5 × 10^{-3}) and extremely large for **8** (Δ_{tun} = 0.22), which allowed the magnetic relaxation to occur *via* the ground states with negligible energy barriers (see Tables S16–S18†). The tunneling gap in the ground state of **2** could be quenched if a certain dc field is applied. In that case, the magnetic relaxation could occur in the 3rd excited states with an energy barrier of 3.7 cm^{-1} (5.3 K). This result corroborates with the experimental observation of **2**. For **5**, the smaller QTM in the ground state and the large TA-QTM in the 16th excited states allowed the relaxation at this higher excited state which lies at 11.1 cm^{-1} (16.0 K). These U_{cal} values of **2** (5.3 K) and **5** (16 K) are also in good agreement with the U_{eff} values of 14.4 K (at 0.14 T) and 31.7 K (at zero dc field) for **2** and **5**, respectively.

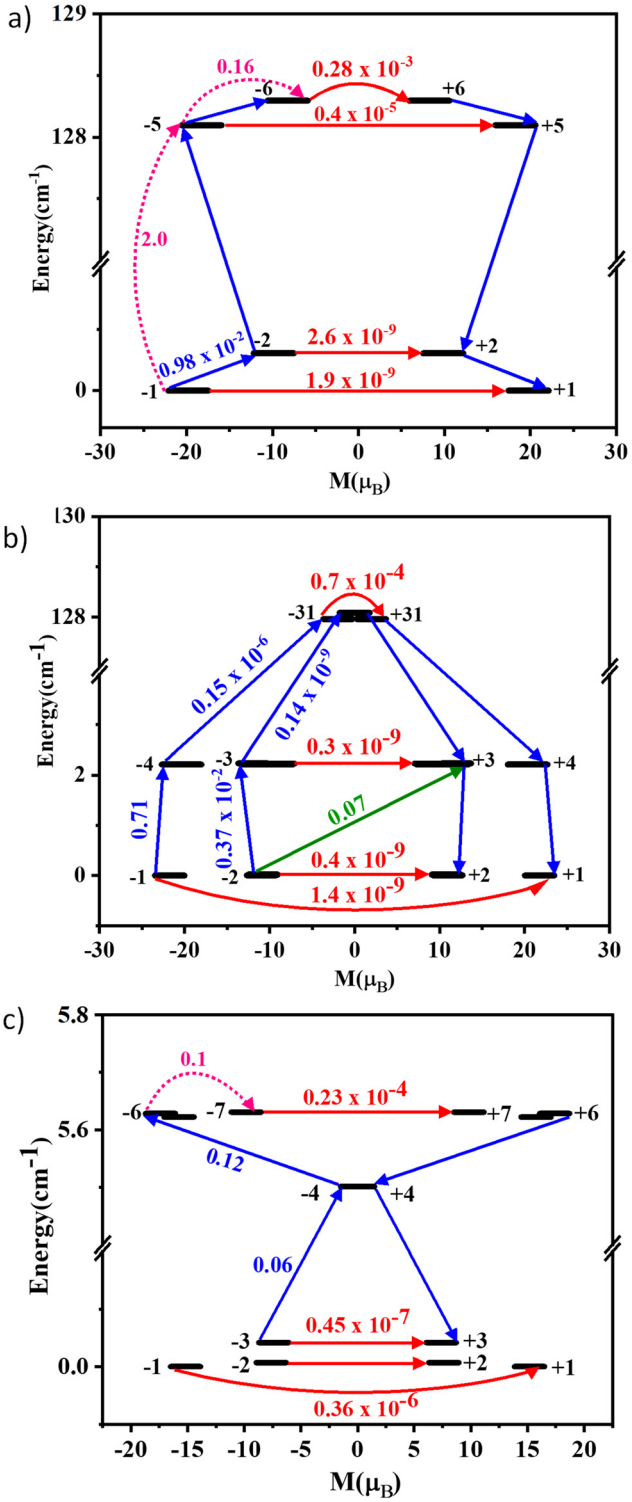

Fig. 6 Low-lying exchange spectra for complexes (a) **1**, (b) **4** and (c) **7** in which exchange states are placed on the diagram according to their magnetic moments (bold black lines). The red arrows show the tunneling transitions (energy splitting) within each doublet state, while the green/blue arrows show the possible pathway through Orbach/Raman relaxation.

In silico design to realize both SMT and SMM behaviors in M_3Dy_3 complexes

All these peroxide bridged complexes **1–9** show an SMM behavior either under an applied dc field or in the absence of a dc field, but they do not show toroidal behavior. Hence, we target to tune these M_3Ln_3 complexes to enhance their SMM properties while also achieving toroidal behavior. To explore this possibility, we modeled a structure (complex **1a**) where the bridged peroxide is simply replaced with a hydroxide in complex **1** (Zn_3Dy_3) and kept other atoms as such in the crystal structure, which yielded intriguing results. We further considered a hydroxide-bridged $[Co_3Dy_3(OH)_4(O_2CCMe_3)_6(teaH)_3(H_2O)_3](NO_3)_2{\cdot}H_2O$ (**10**) SMT, where the experimental studies suggested the presence of a toroidal magnetic state.[30b] We implemented the same computational methodologies that were used for the parent complexes **1–9**, such as CASSCF/RASSI-SO/SINGLE_ANISO/POLY_ANISO calculations, to calculate the single-ion magnetic relaxation mechanism, magnetic anisotropy for each Dy^{III} ion and the exchange coupled states' relaxation mechanism.

Magnetic anisotropic nature and magnetic relaxation mechanism of complexes 1a and 10

The calculated *g*-tensors and the energies of low-lying KDs for each Dy^{III} ion in **1a** and **10** are listed in Table 4. The computed *g*-tensor values are the same for all Dy^{III} centers with a major contribution arising in the main part (g_{zz}) with almost negligible transverse components (g_{xx}, g_{yy}) in **1a**, whereas a small amount of transverse components was observed in ground KD for all the Dy centers in **10**.

The CASSCF computed energies for the low-lying KDs of all Dy centers span in the range of 639–642 cm^{-1} for **1a** and 543–592 cm^{-1} for **10** (see Table 4). The energy gap between the ground and first excited states of the Dy(III) ions ranges from 148.7–153.1 cm^{-1} for **1a** and 46.1–78.6 cm^{-1} for **10**. These low-lying KDs are further grouped according to their transition magnetic moment values to derive the relaxation mechanisms, which are shown in Fig. 7 and S9–S10.† It is observed that the QTM between ground KDs is in the range of 0.0022–0.0036μ_B for Dy ions in **1a** and 0.02–0.12μ_B for Dy ions in **10**. It indicates that the ground KD is a highly pure magnetic state of $m_J = \pm 15/2$ and the magnetic relaxations are likely to occur in the

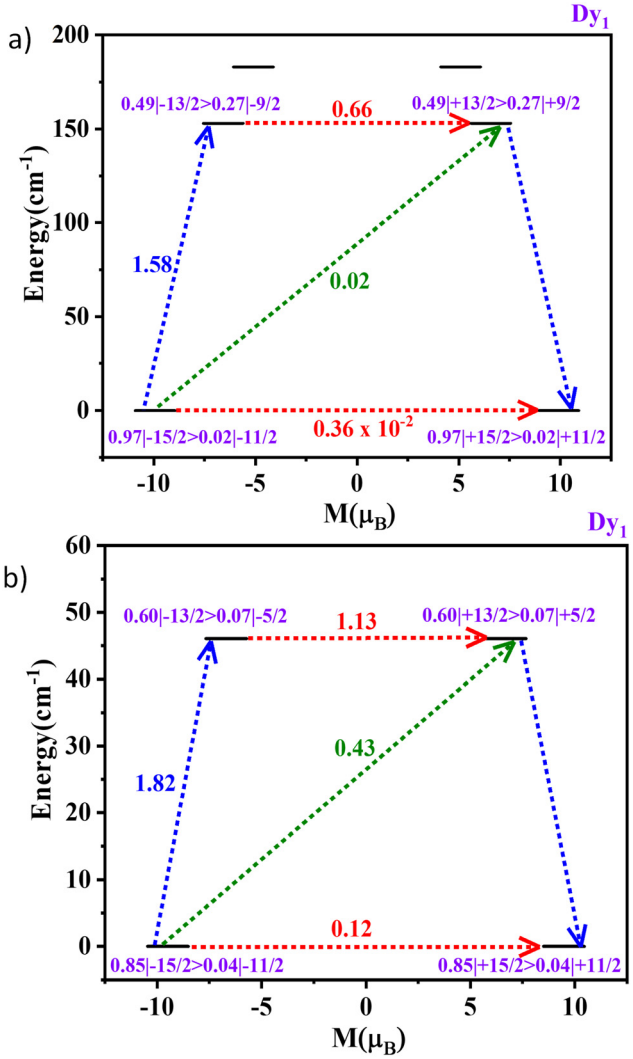

Fig. 7 Magnetization blocking barrier for the Dy1 site in (a) **1a** and (b) **10**. See the Fig. 3 caption for further details.

Table 4 Low-lying energies (cm^{-1}) and *g*-tensors of Dy^{III} fragments that originate from the corresponding ground Kramers doublets in complexes **1a** and **10**

	$\{Zn_3Dy_3\}$ (**1a**)			$\{Co_3Dy_3\}$ (**10**)		
KDs	Dy1	Dy2	Dy3	Dy1	Dy2	Dy3
	0.0	0.0	0.0	0.0	0.0	0.0
	153.1	148.7	150.2	46.1	78.6	69.2
	182.9	183.5	177.3	73.3	109.9	104.1
	240.5	240.3	237.5	112.1	156.8	163.3
	312.2	308.7	307.8	165.6	214.9	224.4
	398.8	391.8	393.8	224.6	294.9	320.3
	549.2	544.5	547.6	333.1	395.1	474.2
	641.5	638.6	641.4	542.7	557.1	591.8
	***g*-Tensor**			***g*-Tensor**		
gx	0.007	0.006	0.004	0.172	0.058	0.027
gy	0.014	0.012	0.008	0.517	0.097	0.046
gz	19.851	19.852	19.852	18.963	19.698	19.784

excited states. Furthermore, the TA-QTM between the first excited states is found to be large and in the range of 1.54–1.58μ_B in **1a** and 1.46–1.82μ_B in **10**. The large TA-QTM values confirm that the single-ion magnetic relaxation can likely occur *via* the first excited state with an energy barrier around 150 cm^{-1} for **1a** and 70 cm^{-1} for **10**.

We have further theoretically examined the ground state toroidal magnetic moment of the $\{Dy_3^{III}\}$ triangle in both complexes **1a** and **10** by predicting the orientation of the g_{zz} axes in the plane of the $\{Dy_3^{III}\}$ triangle. The orientation of the anisotropic axes of all Dy ions is shown in Fig. 8. The anisotropic axes of each $\{Dy^{III}\}$ center are found to lie in the Dy_3 plane with an out-of-plane angle (θ) of 1.39°, 39.26°, and 1.07° for Dy1, Dy2, and Dy3, respectively, in **1a** and 36.1°, 15.29°, and 19.94° for Dy1, Dy2, and Dy3, respectively, in **10**. These out-of-plane angle (θ) values are in the range observed for archetypal triangular $\{Dy_3^{III}\}$ and double $\{Dy_3^{III}\}$ triangular SMTs.[20,23–25] Importantly, these axes follow each other in a circular pattern, which confirms the presence of a toroidal ground state in both complexes. This has been further investigated by computing the LoProp charges of all the donor atoms. The β-electron density (spin-down) of the Dy^{III} ion deviates to reduce the electronic repulsion because of the significant negative LoProp charges on the μ_3-hydroxide bridge (see Fig. 9) and permits all the g_{zz} axes to align between the oxygen of pyridine-2-carboxylate ($PyCO_2^-$) and *N*,*N*′-bis(3-methoxysalicylidene)-1,3-diamino-

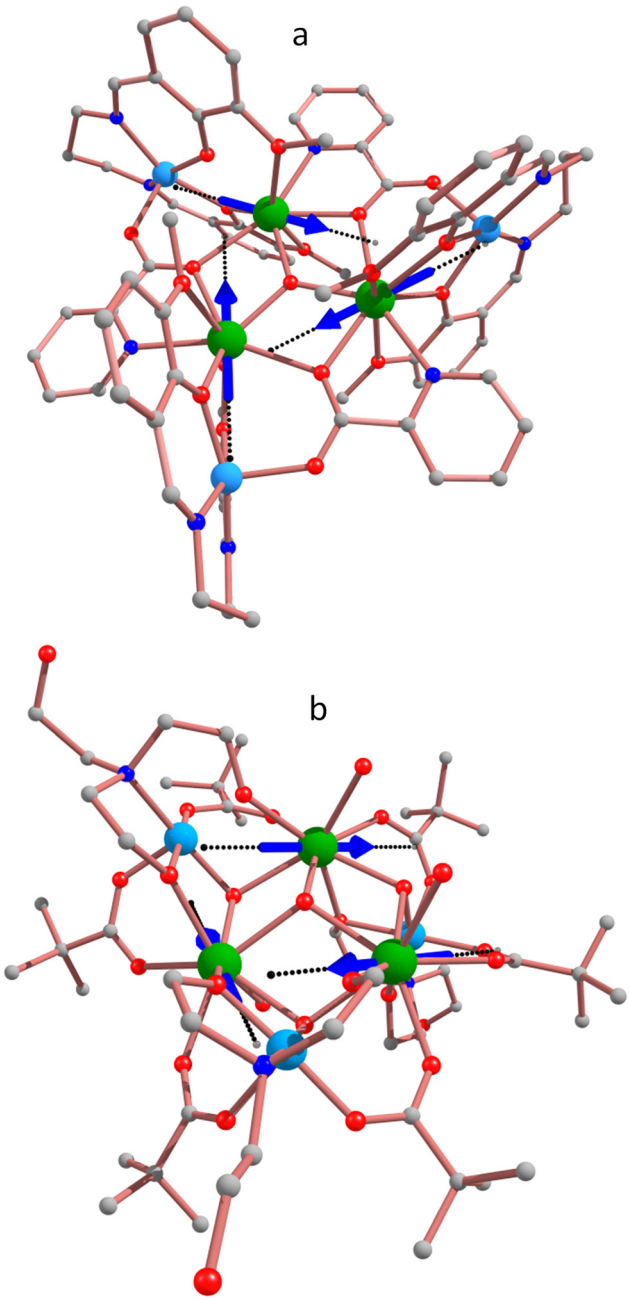

Fig. 8 Orientations of the local magnetic moments in the ground doublet of Dy(III) ions in complexes (a) **1a** and (b) **10**. The blue arrows show the direction of the local magnetic moments of the Dy^{III} ions in the ground state.

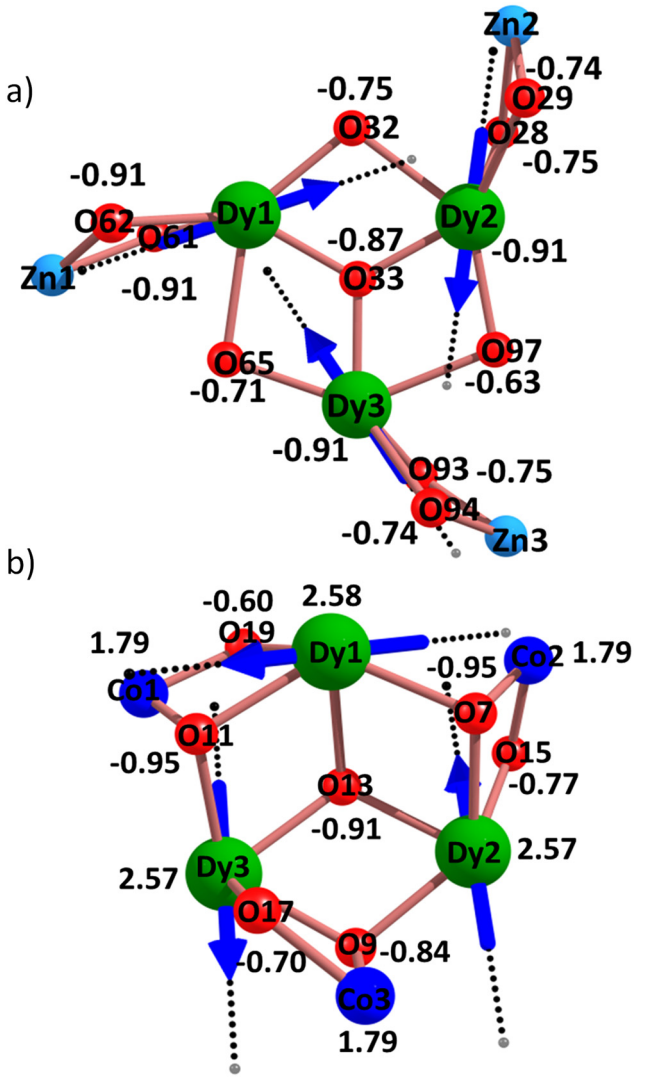

Fig. 9 LoProp charges with the anisotropic directions of Dy(III) ions for complexes (a) **1a** and (b) **10**.

propane (H_2L) ligands in **1a** and triethanolamine (teaH) and pivalic acid (O_2CCMe_3) ligands in **10**. These large negative charges on the hydroxide bridge cause the anisotropic directions to follow each other and form a circular pattern which confirms the toroidal behavior.

These results suggest that the SMT behavior is more feasible through μ_3-hydroxide bridging than through μ_3-peroxide bridging. This could be rationalized considering the larger negative charge on the μ_3-hydroxide bridge in **1a** compared to the μ_3-peroxide bridge in **10**. Furthermore, these μ_3-hydroxide bridges facilitate strong intramolecular magnetic interactions between the Dy ions (see below) and a strong magnetic moment, which are necessary for a complex to exhibit toroidal behavior.[23,24]

Analysis of exchange coupled states' anisotropic barriers of 1a and 10

SINGLE_ANISO calculations confirm the SMM behavior and the toroidal behavior in the ground state for the Dy^{III} metal ions in complexes **1a** and **10**. To gain a deep insight into the relaxation mechanism for the full molecule and to calculate the exchange coupling values between the Dy^{III} metal centers, we used the POLY_ANISO program.[37] We extracted the exchange interactions by fitting the experimentally measured susceptibility data, which yielded a good fit to them (see Fig. 10) and a feasible exchange coupled states' relaxation mechanism (see Fig. 11). The Lines model yielded J values of +0.01 (zJ = 0.001) and +1.85 (zJ = −0.099) between the Dy centers in **1a** and **10**, respectively. In **1a** and **10**, the ferromagnetic exchange between Dy^{III} metal ions led to a very small QTM ($0.15 \times 10^{-3}\mu_B$ for **1a** and $0.44 \times 10^{-3}\mu_B$ for **10**) in the ground exchange coupled state, and a small TA-QTM in the low-lying excited states allowed the magnetic relaxation to occur in the 29th and 9th states, respectively, which yielded energy barriers of 298.6 cm^{-1} and 70.5 cm^{-1}, respectively.

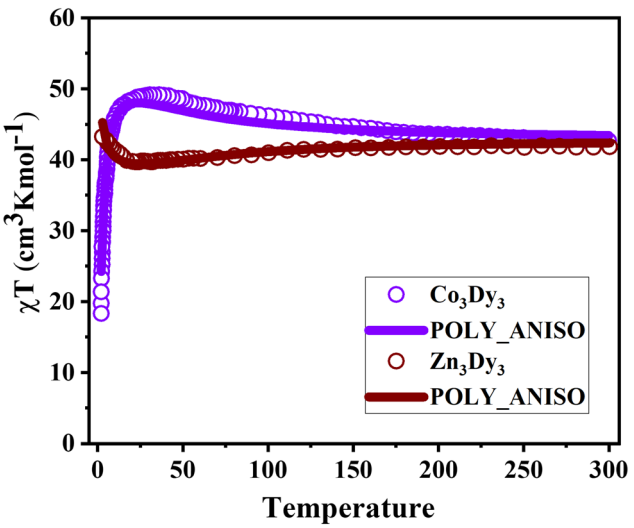

Fig. 10 POLY_ANISO fitted data with the measured magnetic susceptibility data for **10** and **1a**.

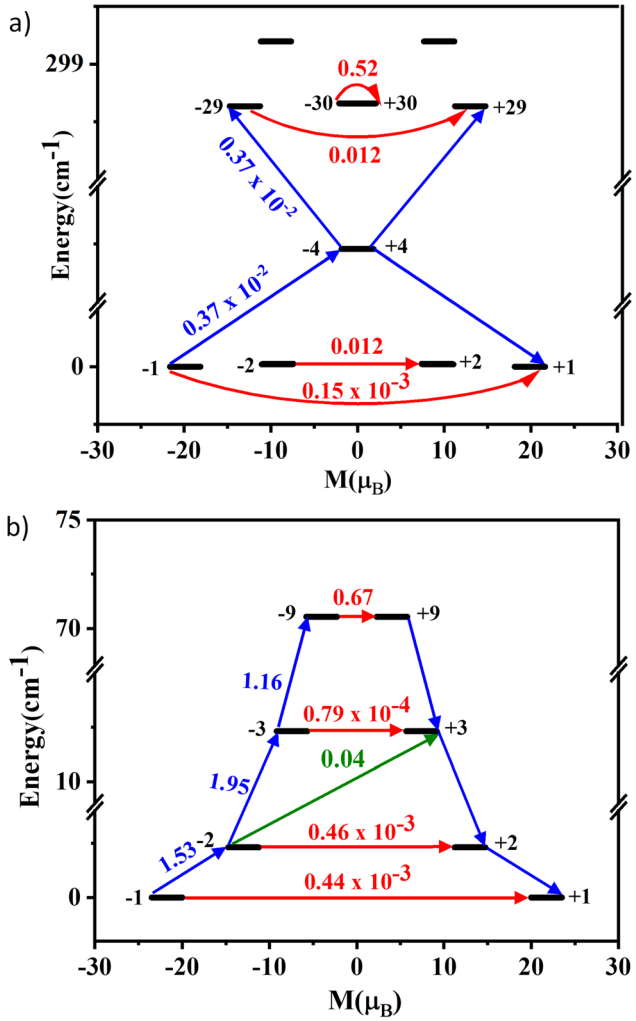

Fig. 11 Low-lying exchange spectra for complexes (a) **1a** and (b) **10**. See the Fig. 6 caption for further details.

Conclusions

Theoretical analysis of nine heteronuclear complexes $\{M_3^{II}Ln_3^{III}\}$ (M = Ni, Cu, and Zn; Ln = Gd, Tb, and Dy) with peroxide bridges was conducted using *ab initio* CASSCF and density functional theory calculations. The goal was to compute magnetic exchange pathways and investigate the origin of SMM and toroidal behaviors in these complexes. The findings from this research are summarised below.

(i) The computational approach of *ab initio* CASSCF + SINGLE_ANISO + RASSI-SO + POLY_ANISO and DFT calculations produced accurate estimates of magnetic exchange constants and experimental energy barriers for all nine complexes, despite their large size.

(ii) All the Dy(III) ions in complexes **1**, **4**, and **7** exhibit extremely small QTM, suggesting that the magnetic relaxation is likely to occur *via* the first excited states and that they can show good SMM behavior. However, the Tb(III) ions exhibit an

extremely large tunneling gap in the ground state itself and they are unlikely to show SMM behavior.

(iii) The simulated magnetic susceptibility data using POLY_ANISO derived J values are consistent with experimental $\chi_M T$ *vs.* T data, supporting the exchange coupled state relaxation mechanism. The U_{cal} values of 184.6 K, 5.3 K, 184.2 K, 16.0 K, and 8.1 K for **1**, **2**, **4**, **5**, and **7**, respectively, are consistent with the U_{eff} values of 126.5 K, 14.4 K, 25.6 K, 31.7 K, and 4.1 K. The overestimation of the U_{cal} value for **2** and **4** is most likely caused by the exclusion of intermolecular and hyperfine interactions from the computation, as well as the potential of a non-Orbach relaxation process.[11,14] These results show that the peroxide-bridged complexes are good SMMs.

(iv) Furthermore, the g_{zz} axis of the Ln centers is aligned along its β-electron density and these anisotropic directions do not follow each other, which indicates the absence of any toroidal behavior. This is attributed to the presence of smaller negative LoProp charges on the peroxide oxygen compared to the peripheral oxygen atoms that deviate from the Ln^{III} ion's β-electron (spin-down) and reduce the electrostatic repulsion. These results show that the peroxide ion is not a good bridge to realize SMT behavior.

(v) However, these peroxide bridges facilitate the ferromagnetic exchange between the Ln ions and the M–Ln ions, which quenches the QTM, lifting the degeneracy of exchange-coupled states and leading to better SMM behavior.

(vi) The model studies on tuning these $\{M_3Ln_3\}$ complexes to enhance their SMM properties while also achieving toroidal behavior, suggesting that the SMT behavior is more feasible through μ_3-hydroxide bridging than through μ_3-peroxide bridging. This could be rationalized considering the larger negative charge on the μ_3-hydroxide bridge in **1a** compared to the μ_3-peroxide bridge in **1**.

(vii) These studied complexes were synthesized using perchlorate metal salts to bring the peroxide ion to the core. We believe changing the perchlorate with nitrate metal salts may lead to different bridges such as oxide or hydroxide, which could certainly affect/improve the magnetic behavior.

In conclusion, the theoretical research conducted here has revealed some significant elements of the magnetic characteristics of $\{M_3Ln_3\}$ complexes, such as how various bridges affect the SMM and SMT properties. As per experimental evidence, the peroxide anion plays a crucial role in the observation of SMM behavior in these $\{M_3Ln_3\}$ heterometallic complexes. However, the peroxide ion does not support the SMT behavior, whereas the hydroxide (OH-) and carbonate (CO_3^{2-}) ions do support the toroidal behavior in $\{M_3Ln_3\}$ complexes.[30]

Data availability

The data supporting this article such as *ab initio* CASSCF computed g-tensors and low-lying energy values of Ln(III) ions, structural parameters of all complexes, crystal-field parameters, POLY_ANISO simulated exchange coupled state energy values with their tunneling gaps, and the *ab initio* computed magnetic relaxation mechanism have been included as part of the ESI.†

Conflicts of interest

There are no conflicts to declare.

Acknowledgements

A. G. thanks the UGC for providing a PhD fellowship. K. R. V. thanks the IISER Mohali-High Performing Computing Facility and Prof. G. Rajaraman, IIT Bombay for providing computing resources, and the SERB for providing start-up research grant funding (SRG/2023/000286).

References

1 (*a*) D. Gatteschi, R. Sessoli and J. Villain, *Molecular nanomagnets*, Oxford University Press, 2006; (*b*) J. M. Frost, K. L. Harriman and M. Murugesu, *Chem. Sci.*, 2016, **7**, 2470–2491; (*c*) R. Sessoli, D. Gatteschi, A. Caneschi and M. A. Novak, *Nature*, 1993, **365**, 141–143.
2 (*a*) E. Coronado and A. J. Epsetin, *J. Mater. Chem.*, 2009, **19**, 1670–1671; (*b*) M. N. Leuenberger and D. Loss, *Nature*, 2001, **410**, 789–793.
3 C. J. Milios, A. Vinslava, W. Wernsdorfer, S. Moggach, S. Parsons, S. P. Perlepes, G. Christou and E. K. Brechin, *J. Am. Chem. Soc.*, 2007, **129**, 2754–2755.
4 J. M. Zadrozny, D. J. Xiao, M. Atanasov, G. J. Long, F. Grandjean, F. Neese and J. R. Long, *Nat. Chem.*, 2013, **5**, 577–581.
5 P. C. Bunting, M. Atanasov, E. Damgaard-Møller, M. Perfetti, I. Crassee, M. Orlita, J. Overgaard, J. v. Slageren, F. Neese and J. R. Long, *Science*, 2018, **362**, 7319.
6 N. Ishikawa, M. Sugita and W. Wernsdorfer, *Angew. Chem., Int. Ed.*, 2005, **44**, 2931–2935.
7 D. N. Woodruff, R. E. Winpenny and R. A. Layfield, *Chem. Rev.*, 2013, **113**, 5110–5148.
8 (*a*) C. A. Goodwin, F. Ortu, D. Reta, N. F. Chilton and D. P. Mills, *Nature*, 2017, **548**, 439–442; (*b*) F. S. Guo, B. M. Day, Y. C. Chen, M. L. Tong, A. Mansikkamäki and R. A. Layfield, *Science*, 2018, **362**, 1400–1403; (*c*) C. A. Gould, K. R. McClain, D. Reta, J. G. Kragskow, D. A. Marchiori, E. Lachman, E. S. Choi, J. G. Analytis, R. D. Britt, N. F. Chilton, B. G. Harvey and J. R. Long, *Science*, 2022, **375**, 198–202.
9 H. D. Li, S. G. Wu and M. L. Tong, *Chem. Commun.*, 2023, **59**, 6159–6170.
10 J. D. Rinehart, M. Fang, W. J. Evans and J. R. Long, *J. Am. Chem. Soc.*, 2011, **133**, 14236–14239.
11 B. S. Dolinar, D. I. Alexandropoulos, K. R. Vignesh, T. A. James and K. R. Dunbar, *J. Am. Chem. Soc.*, 2018, **140**, 908–911.

12 (*a*) J. W. Sharples and D. Collison, *Coord. Chem. Rev.*, 2014, **260**, 1–20; (*b*) T. R. Cook and P. J. Stang, *Chem. Rev.*, 2015, **115**, 7001–7045; (*c*) Y. Peng and A. K. Powell, *Coord. Chem. Rev.*, 2021, **426**, 213490; (*d*) A. Chakraborty, J. Goura, P. Kalita, A. Swain, G. Rajaraman and V. Chandrasekhar, *Dalton Trans.*, 2018, **47**, 8841–8864; (*e*) P. Shukla, S. Das, P. Bag and A. Dey, *Inorg. Chem. Front.*, 2023, **10**, 4322.

13 (*a*) S. K. Langley, D. P. Wielechowski, V. Vieru, N. F. Chilton, B. Moubaraki, B. F. Abrahams, L. F. Chibotaru and K. S. Murray, *Angew. Chem., Int. Ed.*, 2013, **52**, 12014–12019; (*b*) S. K. Langley, D. P. Wielechowski, V. Vieru, N. F. Chilton, B. Moubaraki, L. F. Chibotaru and K. S. Murray, *Chem. Sci.*, 2014, **5**, 3246–3256; (*c*) J. H. Mecchia Ortiz, D. Cabrosi, L. M. Carrella, E. Rentschler and P. Alborés, *Chem. – Eur. J.*, 2022, **28**, e202201450; (*d*) S. K. Langley, D. P. Wielechowski, N. F. Chilton, B. Moubaraki and K. S. Murray, *Inorg. Chem.*, 2015, **54**, 10497–10503.

14 (*a*) S. K. Langley, L. Ungur, N. F. Chilton, B. Moubaraki, L. F. Chibotaru and K. S. Murray, *Inorg. Chem.*, 2014, **53**, 4303–4315; (*b*) K. R. Vignesh, S. K. Langley, K. S. Murray and G. Rajaraman, *Inorg. Chem.*, 2017, **56**, 2518–2532; (*c*) K. R. Vignesh, S. K. Langley, K. S. Murray and G. Rajaraman, *Chem. – Eur. J.*, 2017, **23**, 1654–1666.

15 (*a*) K. R. Vignesh, S. K. Langley, B. Moubaraki, K. S. Murray and G. Rajaraman, *Chem. – Eur. J.*, 2015, **21**, 16364–16369; (*b*) K. R. Vignesh, S. K. Langley, B. Moubaraki, K. S. Murray and G. Rajaraman, *Inorg. Chem.*, 2018, **57**, 1158–1170; (*c*) G. A. Craig, G. Velmurugan, C. Wilson, R. Valiente, G. Rajaraman and M. Murrie, *Inorg. Chem.*, 2019, **58**, 13815–13825; (*d*) A. Mishra, W. Wernsdorfer, K. A. Abboud and G. Christou, *J. Am. Chem. Soc.*, 2004, **126**, 15648–15649; (*e*) C. Papatriantafyllopoulou, W. Wernsdorfer, K. A. Abboud and G. Christou, *Inorg. Chem.*, 2011, **50**(2), 421–423; (*f*) M. Hołyńska, D. Premužić, I. R. Jeon, W. Wernsdorfer, R. Clérac and S. Dehnen, *Chem. – Eur. J.*, 2011, **17**, 9605–9610.

16 (*a*) D. Schray, G. Abbas, Y. Lan, V. Mereacre, A. Sundt, J. Dreiser, O. Waldmann, G. E. Kostakis, C. E. Anson and A. K. Powell, *Angew. Chem., Int. Ed.*, 2010, **49**, 5185–5188; (*b*) C. Schlegel, E. Burzurí, F. Luis, F. Moro, M. Manoli, E. K. Brechin, M. Murrie and J. v. Slageren, *Chem. – Eur. J.*, 2010, **16**, 10178–10185; (*c*) M. A. Roxburgh, S. Zaiter, X. I. Hudson, B. R. Mullaney, J. E. Clements, B. Moubaraki, K. S. Murray, S. M. Neville and C. J. Kepert, *Aust. J. Chem.*, 2017, **70**, 623–631; (*d*) M. A. Hay, A. Sarkar, G. A. Craig, K. E. Marriott, C. Wilson, G. Rajaraman and M. Murrie, *Chem. Commun.*, 2020, **56**, 6826–6829; (*e*) J. L. Liu, J. Y. Wu, Y. C. Chen, V. Mereacre, A. K. Powell, L. Ungur, L. F. Chibotaru, X. M. Chen and M. L. Tong, *Angew. Chem., Int. Ed.*, 2014, **53**, 12966–12970.

17 (*a*) A. K. Ghosh, M. Shatruk, V. Bertolasi, K. Pramanik and D. Ray, *Inorg. Chem.*, 2013, **52**, 13894–13903; (*b*) N. Ahmed, C. Das, S. Vaidya, S. K. Langley, K. S. Murray and M. Shanmugam, *Chem. – Eur. J.*, 2014, **20**, 14235–14239; (*c*) V. Chandrasekhar, P. Bag, W. Kroener, K. Gieb and P. Müller, *Inorg. Chem.*, 2013, **52**, 13078–13086.

18 (*a*) S. K. Langley, B. Moubaraki, C. Tomasi, M. Evangelisti, E. K. Brechin and K. S. Murray, *Inorg. Chem.*, 2014, **53**, 13154–13161; (*b*) A. Worrell, D. Sun, J. Mayans, C. Lampropoulos, A. Escuer and T. C. Stamatatos, *Inorg. Chem.*, 2018, **57**, 13944–13952; (*c*) H. Li, X. Meng, M. Wang, Y. X. Wang, W. Shi and P. Cheng, *Chin. J. Chem.*, 2019, **37**, 373–377.

19 (*a*) S. Roy, P. Shukla, R. Kumar, S. C. Sahoo, T. K. Pal, A. Rajput, J. Klak, M. Hada, K. R. Vignesh and S. Das, *Appl. Organomet. Chem.*, 2022, **36**, e6914; (*b*) A. Upadhyay, C. Das, S. Vaidya, S. K. Singh, T. Gupta, R. Mondol, S. K. Langley, K. S. Murray, G. Rajaraman and M. Shanmugam, *Chem. – Eur. J.*, 2017, **23**, 4903–4916; (*c*) J. L. Liu, Y. C. Chen, Y. Z. Zheng, W. Q. Lin, L. Ungur, W. Wernsdorfer, L. F. Chibotaru and M. L. Tong, *Chem. Sci.*, 2013, **4**, 3310.

20 J. Tang, I. Hewitt, N. T. Madhu, G. Chastanet, W. Wernsdorfer, C. E. Anson, C. Benelli, R. Sessoli and A. K. Powell, *Angew. Chem.*, 2006, **118**, 1761–1765.

21 (*a*) C. Das, S. Vaidya, T. Gupta, J. M. Frost, M. Righi, E. K. Brechin, M. Affronte, G. Rajaraman and M. Shanmugam, *Chem. – Eur. J.*, 2015, **21**, 15639–15650; (*b*) P. H. Guo, J. L. Liu, Z. M. Zhang, L. Ungur, L. F. Chibotaru, J. D. Leng, F. S. Guo and M. L. Tong, *Inorg. Chem.*, 2012, **51**, 1233–1235; (*c*) A. I. Popov, D. I. Plokhov and A. K. Zvezdin, *Phys. Rev.*, 2016, **94**, 184408.

22 (*a*) L. Ungur, S. K. Langley, T. N. Hooper, B. Moubaraki, E. K. Brechin, K. S. Murray and L. F. Chibotaru, *J. Am. Chem. Soc.*, 2012, **134**, 18554–18557.

23 (*a*) K. R. Vignesh and G. Rajaraman, *ACS Omega*, 2021, **6**, 32349–32364; (*b*) L. Ungur, S. Y. Lin, J. Tang and L. F. Chibotaru, *Chem. Soc. Rev.*, 2014, **43**, 6894–6905; (*c*) X. L. Li and J. Tang, *Dalton Trans.*, 2019, **48**, 15358–15370.

24 (*a*) K. R. Vignesh, A. Soncini, S. K. Langley, W. Wernsdorfer, K. S. Murray and G. Rajaraman, *Nat. Commun.*, 2017, **8**, 1023; (*b*) K. R. Vignesh, S. K. Langley, A. Swain, B. Moubaraki, M. Damjanović, W. Wernsdorfer, G. Rajaraman and K. S. Murray, *Angew. Chem.*, 2018, **130**, 787–792; (*c*) J. M. Ashtree, I. Borilović, K. R. Vignesh, A. Swain, S. H. Hamilton, Y. L. Whyatt, S. L. Benjamin, W. Phonsri, C. M. Forsyth, W. Wernsdorfer, A. Soncini, G. Rajaraman, S. K. Langley and K. S. Murray, *Eur. J. Inorg. Chem.*, 2021, 435–444.

25 H. Kaemmerer, A. Baniodeh, Y. Peng, E. Moreno-Pineda, M. Schulze, C. E. Anson, W. Wernsdorfer, J. Schnack and A. K. Powell, *J. Am. Chem. Soc.*, 2020, **142**, 14838–14842.

26 J. D. Rinehart and J. R. Long, *Chem. Sci.*, 2011, **2**, 2078–2085.

27 H. Ke, X. Lu, W. Wei, W. Wang, G. Xie and S. Chen, *Dalton Trans.*, 2017, **46**, 8138–8145.

28 C. M. Liu, D. Q. Zhang, X. Hao and D. B. Zhu, *Inorg. Chem. Front.*, 2020, **7**, 3340–3351.

29 X. T. Wang, H. M. Dong, X. G. Wang, E. C. Yang and X. J. Zhao, *Z. Anorg. Allg. Chem.*, 2016, **642**, 1166–1172.

30 (*a*) J. Goura, E. Colacio, J. M. Herrera, E. A. Suturina, I. Kuprov, Y. Lan, W. Wernsdorfer and V. Chandrasekhar,

Chem. – Eur. J., 2017, **23**, 16621–16636; (*b*) I. Radu, V. C. Kravtsov, S. M. Ostrovsky, O. S. Reu, K. Krämer, S. Decurtins, S. X. Liu, S. I. Klokishner and S. G. Baca, *Inorg. Chem.*, 2017, **56**, 2662–2676.

31 F. Aquilante, J. Autschbach, R. K. Carlson, L. F. Chibotaru, M. G. Delcey, L. De Vico, I. Fdez Galván, N. Ferré, L. M. Frutos, L. Gagliardi, M. Garavelli, A. Giussani, C. E. Hoyer, G. Li Manni, H. Lischka, D. Ma, P. Å. Malmqvist, T. Müller, A. Nenov, M. Olivucci, T. B. Pedersen, D. Peng, F. Plasser, B. Pritchard, M. Reiher, I. Rivalta, I. Schapiro, J. Segarra-Martí, M. Stenrup, D. G. Truhlar, L. Ungur, A. Valentini, S. Vancoillie, V. Veryazov, V. P. Vysotskiy, O. Weingart, F. Zapata and R. Lindh, *J. Comput. Chem.*, 2016, **37**, 506.

32 B. A. Hess, C. M. Marian, U. Wahlgren and O. Gropen, *Chem. Phys. Lett.*, 1996, **251**, 365–371.

33 B. O. Roos and P. Å. Malmqvist, *Phys. Chem. Chem. Phys.*, 2004, **6**, 2919–2927.

34 B. O. Roos, R. Lindh, P. Å. Malmqvist, V. Veryazov, P. O. Widmark and A. C. Borin, *J. Phys. Chem.*, 2008, **112**, 11431–11435.

35 P. A. Malmqvist, B. O. Roos and B. Schimmelpfennig, *Chem. Phys. Lett.*, 2002, **357**, 230–240.

36 L. F. Chibotaru and L. Ungur, *J. Chem. Phys.*, 2012, **137**, 064112–064122.

37 (*a*) L. F. Chibotaru and L. Ungur, *Program POLY_ANISO*, University of Leuven, Leuven, Belgium, 2006; (*b*) M. E. Lines, *J. Chem. Phys.*, 1971, **55**, 2977–2984.

38 L. Noodleman, *J. Chem. Phys.*, 1981, **74**, 5737–5743.

39 M. J. Frisch, G. W. Trucks, H. B. Schlegel, G. E. Scuseria, M. A. Robb, J. R. Cheeseman, G. Scalmani, V. Barone, G. A. Petersson, H. Nakatsuji, X. Li, M. Caricato, A. V. Marenich, J. Bloino, B. G. Janesko, R. Gomperts, B. Mennucci, H. P. Hratchian, J. V. Ortiz, A. F. Izmaylov, J. L. Sonnenberg, D. Williams-Young, F. Ding, F. Lipparini, F. Egidi, J. Goings, B. Peng, A. Petrone, T. Henderson, D. Ranasinghe, V. G. Zakrzewski, J. Gao, N. Rega, G. Zheng, W. Liang, M. Hada, M. Ehara, K. Toyota, R. Fukuda, J. Hasegawa, M. Ishida, T. Nakajima, Y. Honda, O. Kitao, H. Nakai, T. Vreven, K. Throssell, J. A. Montgomery Jr., J. E. Peralta, F. Ogliaro, M. J. Bearpark, J. J. Heyd, E. N. Brothers, K. N. Kudin, V. N. Staroverov, T. A. Keith, R. Kobayashi, J. Normand, K. Raghavachari, A. P. Rendell, J. C. Burant, S. S. Iyengar, J. Tomasi, M. Cossi, J. M. Millam, M. Klene, C. Adamo, R. Cammi, J. W. Ochterski, R. L. Martin, K. Morokuma, O. Farkas, J. B. Foresman and D. J. Fox, *Gaussian 16, Revision C.01*, Gaussian, I., Wallingford, CT, 2016.

40 A. D. Becke, *J. Chem. Phys.*, 1993, **98**, 5648–5652.

41 T. R. Cundari and W. J. Stevens, *J. Chem. Phys.*, 1993, **98**, 5555–5565.

42 (*a*) A. Schaefer, H. Horn and R. Ahlrichs, *J. Chem. Phys.*, 1992, **97**, 2571–2577; (*b*) A. Schaefer, C. Huber and R. Ahlrichs, *J. Chem. Phys.*, 1994, **100**, 5829–5835.

43 (*a*) T. Rajeshkumar and G. Rajaraman, *Chem. Commun.*, 2012, **48**, 7856–7858; (*b*) T. Rajeshkumar, S. K. Singh and G. Rajaraman, *Polyhedron*, 2013, **52**, 1299–1305.

44 S. K. Singh, T. Rajeshkumar, V. Chandrasekhar and G. Rajaraman, *Polyhedron*, 2013, **66**, 81–86.